Hindawi
Advances in Civil Engineering
Volume 2024, Article ID 8312309, 18 pages
https://doi.org/10.1155/2024/8312309

Research Article

Post-Fire Behavior of Modified SIFCON One-Way Plates with Waste Tire Rubber under Flexural Load: Experimental and Numerical Study

Ali M. Hashim and Basil S. Al-Shathr

University of Technology, Baghdad 10011, Iraq

Correspondence should be addressed to Ali M. Hashim; bce.20.02@grad.uotechnology.edu.iq

Received 4 July 2023; Revised 18 November 2023; Accepted 7 December 2023; Published 3 January 2024

Academic Editor: Nicola Buratti

In this research, an experimental and numerical investigation was conducted to study the flexural behavior of modified slurry-infiltrated fiber concrete slurry-infiltrated fibrous concrete (SIFCON) one-way plates after being subjected to a high temperature. The first part is an experimental work to ensure that the model developed is adequate, while the second part is a 3D finite element modeling of the SIFCON plates with the program ABAQUS using a sequentially coupled thermal displacement analysis. The experimental program included testing eight modified SIFCON plates containing waste powder rubber as a partial substitute for natural sand (0%, 5%, 10%, and 15%). All adopted specimens had identical dimensions (1,000 mm length, 300 mm width, and 50 mm thickness). Four specimens were exposed to fire for 2 hr at a constant temperature of 600°C, after which they were rapidly cooled by spraying them with water. Test results showed that increasing the powder rubber content of burned and unburned modified SIFCON specimens decreased the failure load and increased the specimens' ductility factor, as well as the ultimate and service deflections. During the test, the failure of SIFCON was observed to be gradual, and the plates remained in contact even after the ultimate load was attained, whereas the failure of the reference mix (without wasted rubber) was observed to be more rapid than that of other SIFCON mixtures. For the flexural test, it gives desirable strength and good fire resistance. This study provides guidance for the study of SIFCON with waste rubber. Overall, the percentage of error between the experimental and numerical results for the load capacity and midspan displacement was about 5.05% and 8.65%, respectively.

1. Introduction

Slurry-infiltrated fibrous concrete (SIFCON) is a subtype of fiber-reinforced concrete. In the manufacturing of SIFCON, the fibers are first placed into the molds and then infiltrated with cement slurry that normally has a low water-to-cement ratio. This manufacturing technique is distinct from the normal production of fiber-reinforced concrete [1]. The fiber content can be significantly increased by replacing the fibers in SIFCON. Due to the high-strength cement-based matrix and high-fiber content, the energy absorption and post-cracking strength ability, or toughness of SIFCON, can be significantly greater compared to that of traditional steel–fiber-reinforced concrete. The high-fiber content contributes to the relatively expensive cost of SIFCON [2–7].

It has been established that incorporating steel fibers into concrete can increase the material's resistance to cracking. Due to their ability to increase the service life of refractory concrete, steel fibers have been increasingly used over the last 30 years to enhance their performance in a number of applications. Fibers are widely used to increase the ductility of concrete. It has been demonstrated that steel fibers improve the resistance of refractory concrete to spalling [8]. By delaying concrete spalling, it is understood that steel fibers might improve the fire effectiveness of SlFCON elements. Therefore, it contributes indirectly to concrete confinement under compressive stress [9]. Consequently, it is recommended to undertake an experiment to examine SIFCON's performance at elevated temperatures.

Due to a growing vehicle industry and a decline in the quantity and capacity of landfill space, it is becoming increasingly difficult to dispose of waste tires. Currently, 75%–80% of tire debris is buried in landfills. The majority of landfill operations do not allow the disposal of whole tires due to the size of the flames and their propensity to ascend to the surface with time. Investigations have revealed that used rubber tires contain materials that are harmful and do not disintegrate in the environment [10]. Tires can be utilized as aggregates in concrete based on these issues. Aggregate and cement are the two primary materials needed in the construction of buildings using concrete. Despite the fact that 60% of it is considered illegally dumped. The ideal method for getting rid of old tires is to recycle the rubber by mixing it with concrete. The primary objective of investigations relevant to waste rubber has been the substitution of fine aggregate in concrete with waste rubber. Different ratios of recycled rubber replacement in concrete had variable results, and researchers found that 10% crumb rubber replacement is optimal [11]. With a 25% substitution of recycled rubber, the energy absorption of the resultant concrete increases dramatically. However, the compressive strength reduces significantly [12]. The compressive strength decreases proportionately with the amount and size of rubber replacement particles. The decrease in compressive strength may be due to a weakened interfacial transition zone (ITZ) between crumb rubber particles (RPs) and cement material or to elastic modulus variations among rubber and cement [13].

Bisht and Ramana [14] assessed the durability and mechanical properties of concrete containing 0%, 4%, 4.5%, 5%, and 5.5% by weight of recycled tire rubber. The workability of concrete has been seen to decrease when recycled rubber tire content increases. The test results of flexural and compressive strength indicate a slight reduction with 4% substitution of sand by crumb tire rubber. Abrasion resistance and water absorption were also slightly influenced at the identical substitution ratio of crumb tire rubber in concrete. Furthermore, as the replacement level increases, the density of rubberized concrete decreases. This could be due to the increased porosity of the concrete as well as the lower specific gravity of waste tire rubber in comparison to fine aggregates [14].

Ganjian et al. [15] examined the efficacy of concrete mixes containing (5%, 7%, 5%, and 10%) waste rubber tires as cement and aggregate substitutes. The study's findings were as follows: With rising percentages of waste rubber substitution in concrete, compressive strength declined; nevertheless, the reduction in compressive strength at 5% substitution of cement or aggregate with waste rubber was minimal (below 5%), and other concrete parameters were unaffected. Concrete-containing rubber chips as an aggregate replacement have a lower tensile strength than concrete with rubber powder (for cement replacement). The tensile strength decreased by 30%–60% when 5%–10% of aggregate was replaced by chopped tire rubber, whereas the drop for 5%–10% cement substituted by waste powder rubber was 15%–30%. Numerous hydroxyl, carbonyl, and sulfonate groups were introduced by oxidation and sulphonation during the surface modification of recycled tire rubber [15].

The mechanical properties of recycled concrete at various volume fractions of recycled fine aggregates (RFA) substituting natural fine aggregates (NFA) were assessed by Rezaeicherati et al. [16]. Additionally, research was done on how adding colloidal nanosilica particles affected the functionality of both recycled and conventional concretes. The mechanical and physical properties of concrete deteriorate as the volume percent of RFA substituting NFA increases, according to experimental data. Additionally, the mechanical and physical characteristics of ordinary concrete and concrete, including RFA, are improved when the weight percentage of nanosilica replaces cement up to 6%, the optimum percentage of which was determined as 4.5% [16].

A large number of accidental fires have been reported globally in recent years due to the increased application of new concrete trends in the structure of load-bearing elements for towering buildings made up of columns and beams [17, 18]. These structures' fire safety designs have become essential. This is due to the fact that these components' fire resistance for a reasonable amount of time is the last line of defense in case all other attempts to extinguish the fire are unsuccessful [19, 20]. In addition, it is essential to design buildings with the lowest potential danger to both humans and property [21, 22]. The two environmental factors that have the biggest impact on the quality of concrete are the rate of burning and the highest temperature that can be reached. The most damaging causes of heating are the C-S-H phase dehydration, the pore pressure within the cement paste, and the thermal incompatibility of the aggregates and cement paste [23, 24]. High-performance concrete and ultra-high-performance concrete have numerous benefits; nevertheless, these composites are practically brittle while having extremely high compression strength values. The inclusion of enough fibers improves the deformation ability and tensile strength, leading to increased ductility [25, 26]. SIFCON, which will be utilized in strengthening operations and military construction, could be subjected to elevated temperatures due to causes, including fires and explosives. Exposure to high temperatures represents one of the most influential physical degradation factors on the durability of cement-based materials [27].

Olivares and Barluenga [28] examined the burning behavior of high-strength concrete containing waste tires. A small amount of waste rubber aggregate in the concrete mixture reduces the risk of sudden fracturing in high-strength concrete at higher temperatures because water vapor dissipates through the pathways left behind by the combustion of polymeric particles. Furthermore, raising the tire aggregate percentage decreased the temperature and depth of penetration in concrete, and the use of RPs in concrete up to 3% had little impact on the compressive strength despite lowering the stiffness. In their investigation, Marques et al. [29] heated the hardened specimens to 400, 600, and 800°C while replacing 5%, 10%, and 15% of the normal sand in the concrete mixture with waste chopped aggregate. They discovered that the tensile strength, compressive strength, and elastic modulus all declined as the waste aggregate substitute level and temperature increased [29]. Guo et al. [21] evaluated the elastic modulus, compressive strength, stress–strain curve, and toughness at four distinct temperatures in order to

evaluate the impact of high temperatures on the compressive strength of concrete containing steel fibers and chopped rubber. After being subjected to elevated temperatures, both tensile strength and compressive strength decreased, with the decrease being more pronounced at larger chopped rubber percentages [30].

Aslani and Klein [31] studied fiber-reinforced self-compacting concrete with lightweight aggregate and crumb rubber. They found that when the temperature went up, the tensile strength of concrete reinforced with steel fibers dropped less than that of concrete reinforced with PP fibers. In addition, after being exposed to 600°C, the elastic modulus of the specimens decreased by an average of 50%. Bengar and Shahmansouri [32] studied the compressive behavior of rubberized concretes that were enclosed in steel tubes, where rubber replaced fine particles to varying degrees (0%, 7.5%, and 15%). After heat loading at 200, 400, 600, and 800°C. Thirty specimens underwent mechanical testing. Experimental research was done on the post-fire physicomechanical characteristics, including compressive strength, failure mode, elastic moduli, stiffness, compressive stress–strain relationship, and peak strain. The experimental results show that a temperature rise of up to 400°C has no discernible impact on the compressive strength of rubberized steel tube-confined concrete, but a temperature increase of up to 800°C causes a discernible drop in the compression of the specimens. Moreover, raising the exposure temperature and waste rubber substitution content causes an increase in the steel tube-confined rubberized concrete's peak strain. After heating at different temperatures, Tang et al. [33] studied the properties (compressive strength and peak strain) of rubber-modified recycled aggregate (RA) concrete that had different amounts of RA and recycled RPs. The concrete was heated at different temperatures. The results show that elevated temperatures significantly reduced uniaxial compressive strength, though adding RA (for example, 50%) and RPs (for example, 5%) can lessen the negative effects of elevated temperatures. Increasing the replacement ratios of RP and RA could possibly enhance the peak strain.

2. The Aim of Study

SIFCON is a newly developed construction material, and limited information on SIFCON behavior under fire effects is known from previously published research. From this point of view, this study tried to experimentally investigate the behavior of modified SIFCON plates by partial substitution of normal sand with recycled tire rubber under flexural loading prior to and after fire exposure. In addition, the load–displacement behavior of SIFCON plates was evaluated, along with failure modes and visual observations.

3. Methodology

3.1. Materials Used and Mix Proportions. Ordinary Portland cement Type I in accordance with ASTM C150-18 [34] standards was used. Cement had a specific gravity of 3.15, an initial setting time of 98 min, and a final setting time of 177 min. Sand from a natural river has a maximum particle size of 0.60 mm. The specific gravity of the fine aggregate was determined to be 2.65, the free surface moisture to be 1%, the water absorption to be 1.5%, and the fineness modulus to be 2.83. It has to be sufficiently fine to ensure complete penetration through the dense steel fiber without clogging. Table 1 shows the sieve analysis of the used sand. A polycarboxylate-based superplasticizer, which complies with ASTMC494/C494M-17 [35], was used in order to produce the requisite workability of the slurry, which must be sufficiently fluid to pass through the thick fiber bed without causing honeycombs. Furthermore, a hooked-end steel fiber with a length of 35 mm, a diameter of 0.5 mm, and an aspect ratio of 70 with a tensile strength of more than 1,100 MPa was utilized in this study. The steel fiber volume fraction employed in this investigation was 4%. The fiber volume was determined depending on the volume of each specimen's mold. The hooked-end steel fiber used in the present investigation is shown in Figure 1.

Table 1: The sieve analysis of the used sand.

Sieve size (mm)	Passing by weight (%)
4.75	100
2.36	100
1.18	100
0.60	100
0.30	41
0.15	11

Figure 1: The steel fibers used.

A local industry collected waste rubber. After removing the steel and textile fibers, the waste rubber was ground into powder, which was sieved using a 0.6-mm sieve. When replacing, the specific gravity difference between river sand and waste rubber was considered. The replacement mass of fine aggregate was calculated by multiplying the ratio of rubber's specific gravity to that of sand. Rubber powder has a specific gravity of 1.05. The powder rubber used in this investigation is shown in Figure 2. Powder rubber replaced natural sand at different percentages (5%, 10%, and 15%) by weight. About 10% microsilica by weight of cement was added to the SIFCON, complying with the requirements of ASTM C1240-15 [36] to improve the ITZ bonding. Silica fume may increase the strength of concrete by providing dense packing and by filling the pores of cement paste [37].

Figure 2: The waste rubber tires used.

Table 2: Fresh properties of SIFCON mortar.

Mortar symbol	Water/binder ratio	HRWR (%) by wt. of cement	V-funnel (s)	Mini slump flow (mm)
M1	0.26	2.7	8.5	258
M2	0.26	2.9	9	256
M3	0.26	3.3	10	255
M4	0.26	3.7	11	254

Table 3: SIFCON matrix of reference mix.*

Constituent	Mix proportion
Cement (kg/m^3)	872.4
Natural sand (kg/m^3)	969
SF (kg/m^3)	96.9
Hooked end steel fiber (kg/m^3)	312

*The ratio of sand to cementitious materials is 1 : 1.

Table 2 shows the results of the mini-slump flow and V-funnel test following ASTM C1437 [38] that satisfied the criteria of acceptable flow ability, appropriate viscosity, and filling ability for the four SIFCON mortars M1, M2, M3, and M4 for 0%, 5%, 10%, and 15% powder rubber replacement, respectively. The findings of the SIFCON mortars show that the inclusion of high-range water reducers (HRWR) is crucial for achieving a mix with a low w/b ratio while still meeting homogeneity and other parameters. It was established that this substitution reduces the mix's workability, making it cohesive and sticky. As a result, the HRWR dose of the mixture must be raised to achieve equivalent viscosity and fluidity. The results show that adding powder rubber reduces the spread width of the slump flow and extends the V-funnel time. In other words, replacing rubber with powder generates a high level of viscosity. This is caused by their irregular shape and sharp edges [39, 40], which noticed that the spread diameter of the slump flow and the volume of slurry that penetrated the fiber mass decreased with the higher dose of powder rubber. Table 3 lists the SIFCON mix design.

3.2. SIFCON Plates. SIFCON plates of 1,000 mm × 300 mm × 50 mm were prepared for each mix using wooden molds, as shown in Figure 3. These dimensions were chosen to simulate the practical site conditions where SIFCON plates are usually used in the repair and strengthening of damaged concrete beams due to bending failure. The experimental study involved evaluating eight SIFCON plate specimens that had been cast in the laboratory and tested under a four-point bending test (known as a two-line load). Four SIFCON plate specimens that were not subjected to fire were compared with the reference group of four plates that were exposed to fire. After 28 days of water curing, the plates were coated with white paint to get a clear view of the crack patterns. The SIFCON plate was subjected to two-point loading, as shown in Figure 4, using a hydraulic compression machine with a capacity of 500 kN and a stress rate of about 1.0 kN/10 s. The deflection of the plate models was determined using three linear variable displacement transducers (LVDTs). One of these three LVDTs was placed at the center point of the specimen, and the other two LVDTs were placed at the one-third point of the longitudinal direction, as shown in Figure 5. These LVDTs were supported in a way so they could touch the lower surface of the models. Table 4 represents the symbols of all mixtures that were examined in this study and that appear in the tables and figures of the study's results.

3.3. Burning Procedure of the Specimens. The primary purpose of the fire-flame furnace is to heat SIFCON plates to the intended temperature and maintain the temperature for specified time periods. Figure 6 illustrates the furnace and equipment details. The dimensions of the furnace are 2.9, 0.9, and 1.0 m in length, width, and height, respectively. The wall thickness is fixed at 200 mm on all sides, as illustrated in Figure 6. The burner's network consists of eight methane burners coordinated in one line at the lower side of the furnace (four methane burners for each SIFCON plate). All

Figure 3: Casting of SIFCON plates.

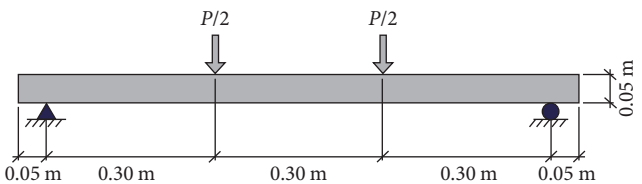

Figure 4: Dimensions and details of SIFCON plate specimens.

methane burners were connected to the main pipeline in order to control gas discharge and to the container of gas. The aim of the fire flame bars was to simulate the heating conditions in a realistic fire. A digital gauge was connected to thermocouples and the electric gas regulator in order to regulate the liquid petroleum gas. A thermocouple is often linked by thermally insulated electric wire to a thermometer or other thermocouple-capable device (digital gauge utilized

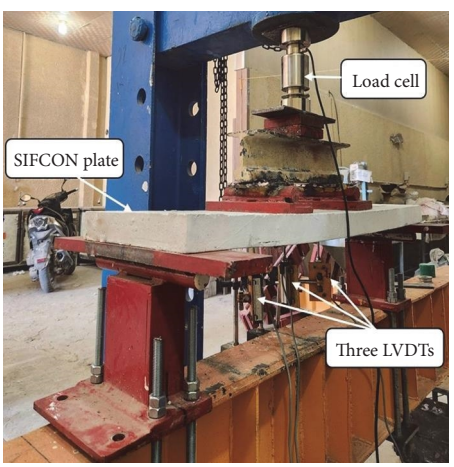

Figure 5: Testing procedure for SIFCON plates.

Table 4: Codes of the samples.

Sample code	Steel fiber (%)	Sand replacement by powder rubber (%)
M1-F4	4	0
M2-F4-P5	4	5
M3-F4-P10	4	10
M4-F4-P15	4	15

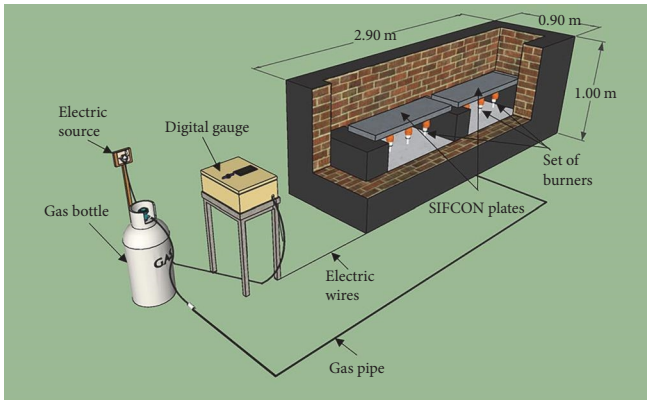

Figure 6: The furnace and equipment.

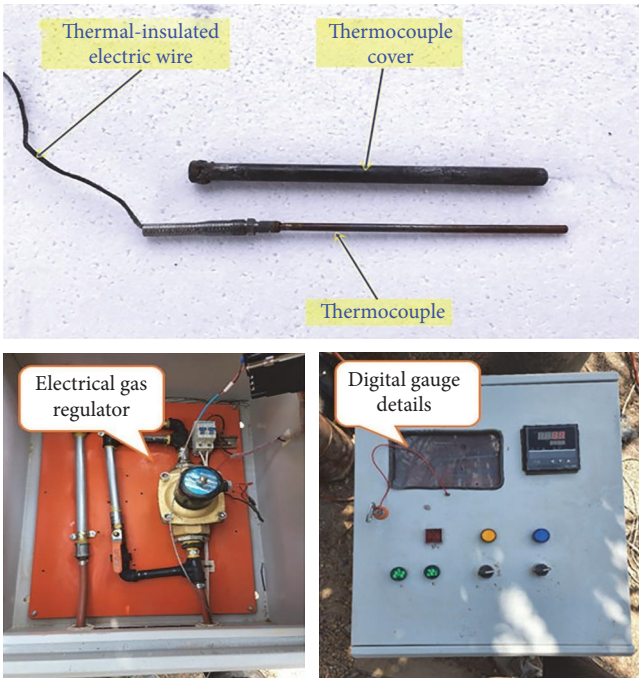

Figure 7: Thermocouple and digital gage details.

in this study) to resist elevated temperatures during combustion. Figure 7 illustrates the digital gauge and thermocouple in detail.

As shown in Figure 8, the SIFCON plate specimens were burned in the furnace in accordance with the provided ISO-834 standard time–temperature curve. Up to 600°C, the initial portion of the fire curve was comparable to the standard fire curve. SIFCON plates were maintained at this maximum

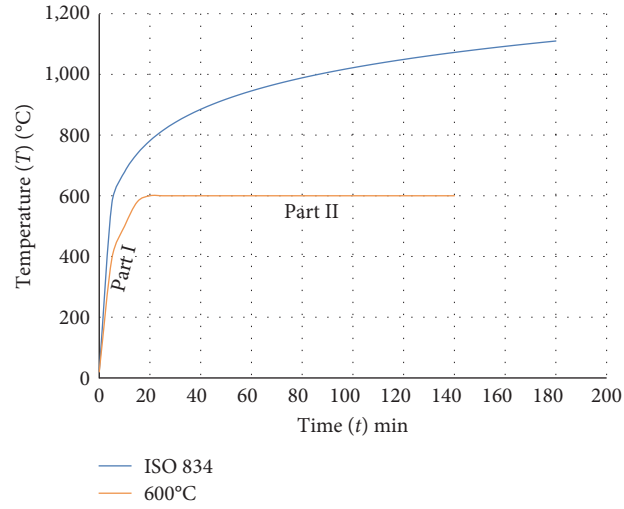

Figure 8: Experimental and ISO-834 standard recommended temperature–time curves.

temperature of 600°C for 2 hr after achieving the specific fire temperature (as shown in Part I in Figure 8). After that, SIFCON samples were cooled down in a laboratory condition.

The MATLAB software programed the real-time temperature curve. Then, the heated thermocouple within the furnace could be linked to the computer and used to record temperature data that was directly correlated with time. After that, when the burning process is complete, the data on temperature and time is stored on the computer, along with the final shape of the time–temperature curve. The time–temperature curve in Figure 9 was drawn using the computer program MATLAB as an example.

4. Finite Element Analysis (FEA)

In this research, a 3D nonlinear numerical analysis has been carried out to simulate the post-fire behavior of SIFCON plates using the FEM program ABAQUS. In general, the process includes three main phases are as follows:

(i) Phase A: modeling and simulating the reference samples (unfired plates).
(ii) Phase B: modeling and simulating the SIFCON plate samples subjected to high temperatures.

4.1. PHASE A: Modeling of Reference Concrete Beam Samples

4.1.1. Geometrical Modeling. Abaqus provides a flexible platform for modeling in addition to its ability to import parts from other software, such as AutoCAD, with suitable and various file extensions. Generally, the procedure followed for geometrical modeling was to create parts individually according to their types: 3D, 2D, or 1D part. Moreover, some of the parts are deformable, and some others are rigid parts according to the simulation status.

For SIFCON plates, 3D deformable parts were used using the extraction procedure, which, in brief, the cross-section of

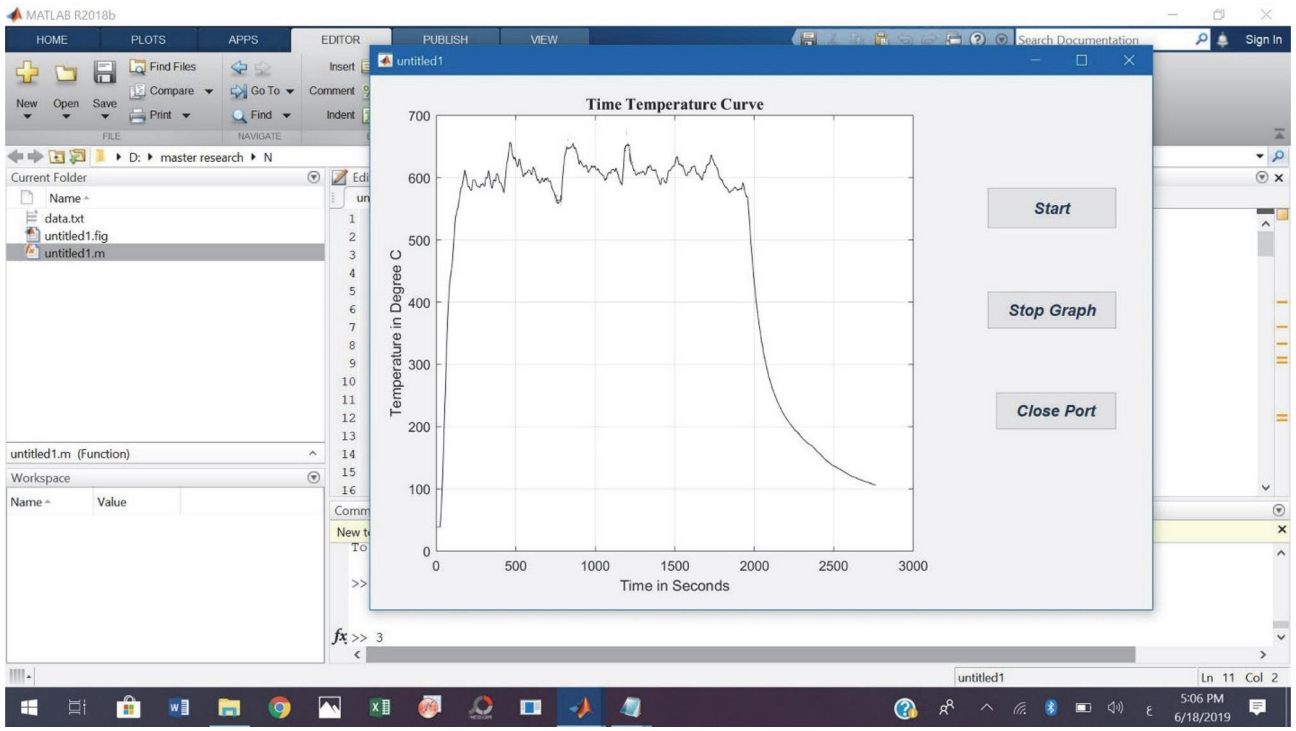

Figure 9: An illustration of how a MATLAB program records and draws a time–temperature curve.

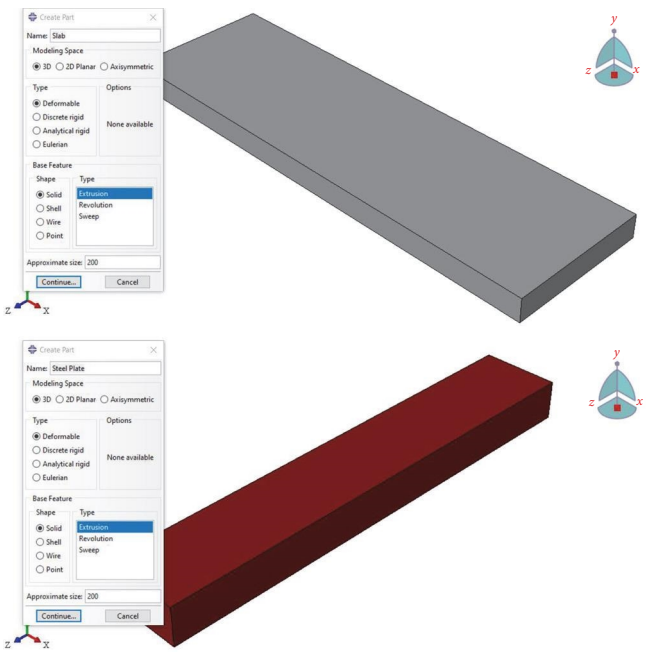

Figure 10: Parts geometrical modeling.

the plate is drawn in XY plane, and then a suitable extraction length is assigned to each part. This method is most commonly used for 3D parts having straight longitudinal profiles. Figure 10 illustrates the adopted procedure for geometrical modeling of various parts.

4.1.2. Materials Models and Assigned Section. Abaqus provides various material properties that reflect their behavior under different simulation conditions. Moreover, different failure theories are provided for metals, soils, concrete, etc. To simulate concrete elements, it is commonly used to define two phases: elastic and plastic phases. The elastic phase for isotropic materials is commonly characterized by two parameters: modulus of elasticity and Poisson's ratio. There are two models used to characterize the concrete plastic phase: the concrete damaged plasticity (CDP) model and the concrete smeared cracks model. Most researchers recommended using the CDP model to characterize the plastic phase of quasi-brittle materials such as concrete because of its efficiency to predict concrete response under various conditions, such as monolithic and repeated loadings, plain and reinforced concrete, and applications those depend on materials loading rate.

4.1.3. Assembling Parts. Assembling means collecting the created parts into the simulation environment using an assembly module. The inserted parts are then called instances. In this module, instances are created, translated, rotated, or duplicated according to the required simulation. Figure 11 illustrates part assembling of the SIFCON plate.

4.1.4. Analysis Procedure. Abaqus provides various types of analysis suits for different engineering applications called steps. The static step suits most engineering applications where the loading frequency is less than 1/3 the structure's natural frequency or when the kinetic energy is less than 5% of the internal energy. Beyond such limit, the quasi-static analysis is required to perform. Abaqus library includes a heat transfer analysis procedure and coupled thermal-displacement analysis to capture the coupled effect of mechanical and thermal loading on the structure. In this study, the static analysis

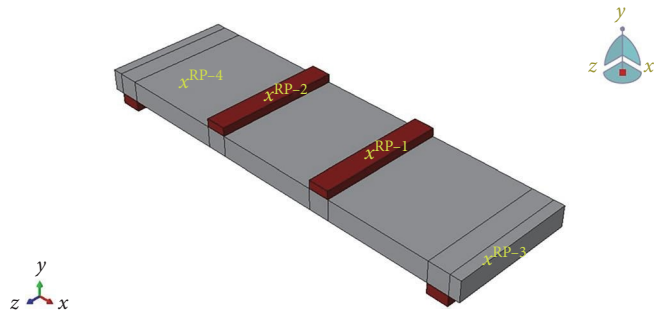

Figure 11: Part assembling of the SIFCON plate.

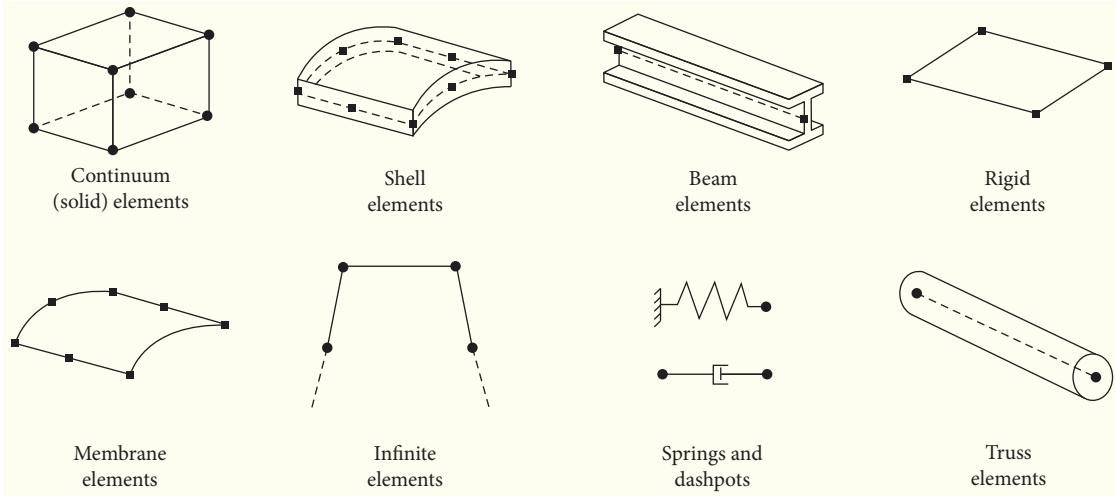

Figure 12: Element type's library in Abaqus [41].

procedure has been adopted to solve the SIFCON plates those are not subjected to fire. While to investigate the thermal distribution on the plate cross section, the heat transfer analysis procedure was used. Other SIFCON plates those are tested after exposing them to fire are analyzed with the static analysis step.

4.1.5. Meshing Properties. The meshing technique is the method of segmenting and converting the simulated parts into smaller ones using different shapes and division algorithms. The produced parts are then called elements. In general, different types of elements are provided in the Abaqus library, as can be seen in Figure 12 [41]. A continuum solid element was used for 3D parts (test machine plates and SIFCON plates), 3D stress family, and brick (hexagonal) shape (C3D8R).

The structural mesh algorithm technique was used to generate mesh distribution. The dimension of concrete elements (brick, eight nodes, reduced integration) was 20 mm × 20 mm × 20 mm. Figure 13 illustrates the generated mesh for the SIFCON plates.

4.2. Phase B: Modeling the Thermal Distribution on SIFCON Samples

4.2.1. Geometrical Modeling and Assembling. The same techniques and dimensions used in Phase A are used in this stage.

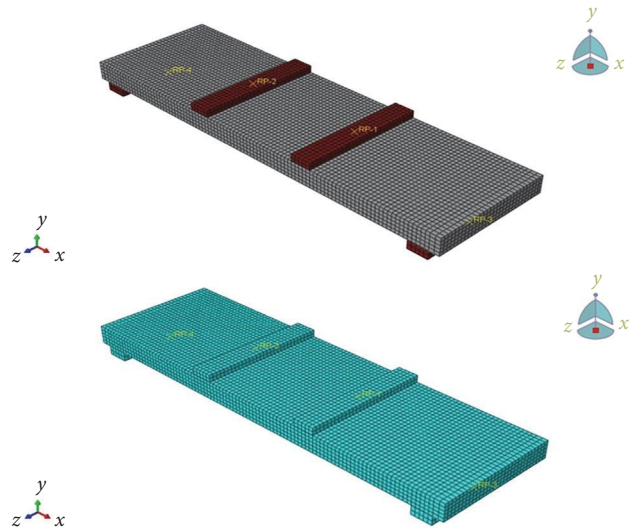

Figure 13: Meshing of the SIFCON plates using structural mesh algorithm techniques.

4.2.2. Material Properties. Like other materials, when concrete is subjected to fire at high temperatures, the strength of the material starts to degrade proportionally due to its nature. The chemical bonding of cement mortar in addition

Table 5: Ultimate load, deflection, and flexural strength of all SIFCON plates.

Specimen	At 25°C			At 600°C		
	First crack load (Pcr) (kN)	Ultimate load (Pu) (kN)	Pcr/Pu (%)	First crack load (Pcr) (kN)	Ultimate load (Pu) (kN)	Pcr/Pu (%)
M1-F4	15.2	25.3	60.5	14	21.1	66
M2-F4-P5	10.9	22.1	49.3	8.6	13.5	63.7
M3-F4-P10	10.5	21.3	49.2	8.2	13	63
M4-F4-P15	9.1	18.9	48.5	6.4	11.1	57.6

Table 6: Middle-third deflections of SIFCON plates at service and ultimate load at 25°C.

Specimen	The control specimen deflection at service load level (mm)	Percentage increase in deflection at service load (control specimen)	Deflection at ultimate load (mm)	Percentage increase in deflection at ultimate load (control specimen)
M1-F4	6.46	—	12.48	—
M2-F4-P5	9.09	40.7	12.91	3.4
M3-F4-P10	9.3	43.9	14.2	13.7
M4-F4-P15	11.01	70.4	13.8	10.6

to the expansion of the components. Therefore, it is necessary to characterize the thermal properties of such concrete types since they are required as input data to Abaqus for heat transfer analysis. Generally, it is necessary to define concrete thermal properties such as thermal connectivity, density, and specific heat of concrete.

4.2.3. Meshing Techniques and Type Element Solver Library. The same mesh techniques, element shape, and size used in Phase A for SIFCON are used in this phase except for the element solver library (element degree of freedom). The selected element solver family was heat transfer for the SIFCON elements, which has only the thermal degree of freedom.

5. Results and Discussion

5.1. Control SIFCON Specimens. The test results of the first crack load and ultimate load for all SIFCON mixes at temperatures of 25 and 600°C are presented in Table 5. For all tested plates, the failure mode was flexure. The center third of the tension face of the plate, which is where the largest moment occurred, was where the first flexural cracking initially appeared. Further load increases led to the generation and extension of new flexural cracks parallel to the original crack's path and the direction of the supports on the plate's bottom surface. No cracks were seen close to the supports, and cracks were observed in the middle portion of the plate. It is obvious that the crack pattern is almost similar in all SIFCON specimens. Additionally, during the test, the failure of SIFCON was gradual, and the plates remained in contact even after the ultimate load was reached, whereas the failure of the reference mix (without waste rubber) was observed to be faster than that of other SIFCON mixes.

The first cracks for the four non-burned SIFCON specimens ranged in magnitude from 9.1 to 15.2 kN and appeared between 48.5% and 25.3% of their ultimate load capacity. As shown in Table 5, the control SIFCON plate M1-F4's first flexural crack appeared at a load of 15.2 kN. The first cracking load is reduced to 10.9, 10.5, and 9.1 kN for specimens M2-F4-P5, M3-F4-P10, and M4-F4-P15, respectively. As a result, the SIFCON specimens' resistance to cracking decreases as the ratio of sand replacement with waste powder rubber rises. For plates M2-F4-P5, M3-F4-P10, and M4-F4-P15, the corresponding percentage reductions in initial cracking with respect to control specimens are 28.3%, 31%, and 40.2%, respectively. Additionally, it is clearly shown in Table 5 that the control specimen M1-F4's load capacity (ultimate load) is 25.3 kN. While using powder rubber as a partial replacement for sand (specimens M2-F4-P5, M3-F4-P10, and M4-F4-P15), the ultimate loads were 22.1, 21.3, and 18.9 kN, respectively. In general, it is clear from the results that raising the powder rubber proportion decreased the failure load. The percentage reduction was 12.7%, 15.9%, and 25.3% for specimens (M2-F4-P5, M3-F4-P10, and M4-F4-P15) with respect to the control specimen (M1-F4).

Table 6 shows the central deflection results of SIFCON plate specimens at service and ultimate load stages at 25°C. LVDT equipment and a data logger installed for recording the deflection and load data each second through the load test are used to determine the vertical deflection in the center of the SIFCON plates. At two load levels, the behavior of SIFCON specimens with sand that has been partially replaced with powder rubber is compared to that of the control specimen.

Stage one: Service load stage. It is important to note that, according to Tan and Zhao [42], the service load limit is approximately 70%–75% of the maximum load. Therefore, it is assumed that the service load is 70% of the ultimate load of the control specimen (M1-F4). When compared with the control specimen M1-F4, at the same load level as the control specimens, the effect of using powder rubber on increasing the deflection at service load is relatively adequate, increasing

Table 7: Middle-third deflections of SIFCON specimens at service and ultimate load at 600°C.

Specimen	The control specimen deflection at service load level (mm)	Percentage increase in deflection at service load (control specimen)	Deflection at ultimate load (mm)	Percentage increase in deflection at ultimate load (control specimen)
M1-F4	5.8	—	11.15	—
M2-F4-P5	—	—	9.69	13.1
M3-F4-P10	—	—	10.27	7.9
M4-F4-P15	—	—	10.82	2.9

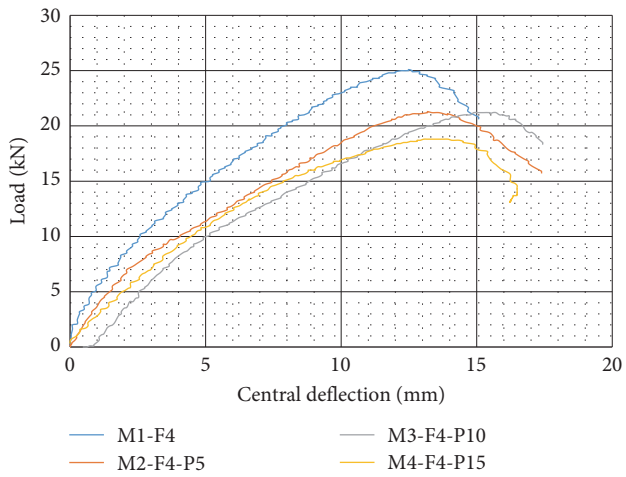

Figure 14: Load-central deflection behavior for SIFCON plates tested at 25°C.

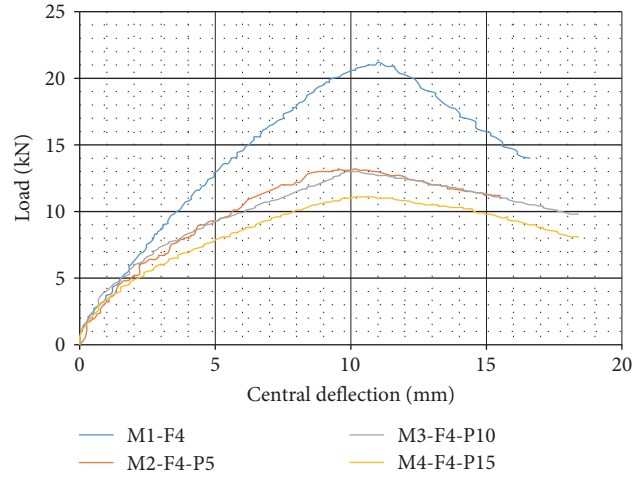

Figure 15: Load-central deflection behavior for SIFCON plates tested at 600°C.

by 40.7%, 43.9%, and 70.4% for specimens M2-F4-P5, M3-F4-P10, and M4-F4-P15, respectively.

Stage two: The ultimate load stage. As the load was raised, the deflection developed quickly following the initiation of the first crack. As the cracks formed, the deflection continued to rise without a noticeably higher load until failure, as seen in Figure 14. In general, it can be said that SIFCON plates with powder rubber have more ductility at room temperature than SIFCON plates without rubber.

5.2. Burned SIFCON Specimens. Tables 5 and 7 show the results for SIFCON specimens that were burned at 600°C. The experimental investigation showed that cracks appeared on the plates' surfaces after firing and cooling, and flexural cracks also appeared as a result of fire and applied loads on the bottom and sides of the plates. The specimens were tested under two line loads of static load after the burning and cooling processes were finished.

Flexural failure occurred for all SIFCON plates. At first, cracks appeared at the bottom of the plate (new cracks), which also developed from fire cracks on the plate's bottom side. The ultimate load of the plate is clearly lowered by fire; the residual ultimate load was 83.3% for the reference specimen M1-F4. While the residual ultimate loads for specimens M2-F4-P5, M3-F4-P10, and M4-F4-P15 were 61.08%, 61.03%, and 58.73%, respectively. So, increasing the ratio of sand replacement to waste powder rubber results in a decrease in the fire endurance of the SIFCON plates. The width of the critical crack generally reduces with an increase in powder rubber content, which results in a more dispersed crack distribution. This is primarily caused by the well-known vapor pressure mechanism, which significantly degrades the bonding between aggregates and cement paste when moisture in the concrete evaporates following being subjected to elevated temperatures. For the rubberized concrete, however, the rubber melts, and the internally connected pores are created at a temperature of 170°C or higher, allowing for the passage of the vapor. As a result, the damage caused by interior vapor pressure may be greatly reduced. Microcracks begin along the cement–paste aggregate interface as a result, and they may coalesce into macrocracks during the test. As a consequence, the damage to the concrete structure before the test might have been minimal; therefore, the microcracks in rubberized concrete may have been primarily caused by the testing effect. Wide and deep macrocracks are observed in specimens M2-F4-P5, M3-F4-P10, and M4-F4-P15 that have been exposed to elevated temperatures. This is most likely because the enormous space or void created by the melted rubber on the plate structure has caused more damage than benefit by lowering the water vapor pressure, making the SIFCON plate less resistant to cracking during testing.

After being exposed to fire, the SIFCON plate specimens' load deflection changed, as illustrated in Figure 15. The results reveal that, in comparison to those of SIFCON plates that had

Figure 16: Photos of SIFCON specimen surface after exposure to a fire flame at 600°C.

Table 8: Finite element results of all SIFCON plates.

Specimen	At 25°C		At 600°C	
	Deflection at ultimate load (mm)	Ultimate load (Pu) (kN)	Deflection at ultimate load (mm)	Ultimate load (Pu) (kN)
M1-F4	14.9	26.8	11.3	23.3
M2-F4-P5	15.7	22.6	13.3	14.5
M3-F4-P10	15.4	21.9	10.6	13.4
M4-F4-P15	15	19.2	8.4	11.9

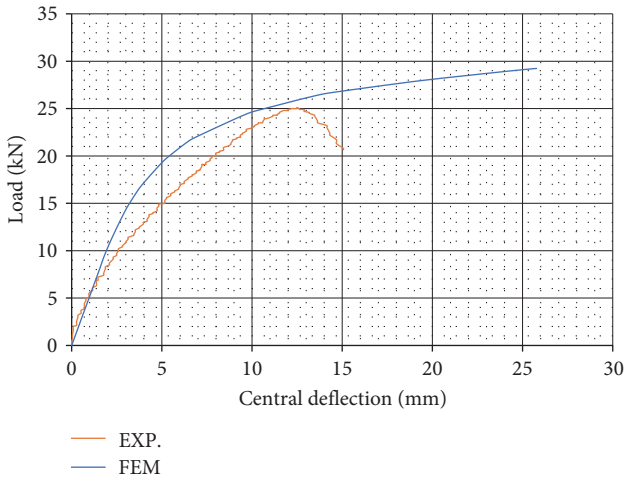

Figure 17: Load–displacement curves' comparison between the FEM and the experimental work results for M1-F4.

not been burned, the center deflection of the SIFCON plates increased in proportion to the magnitude of the applied load, and the load deflection of the SIFCON plates showed smoother behavior, as shown in Figure 11. This might be attributable to the relative loss of stiffness of SIFCON plates exposed to fire (particularly for SIFCON plates with powder rubber replacement), which was primarily caused by the loss of SIFCON's elastic modulus and the development of cracks.

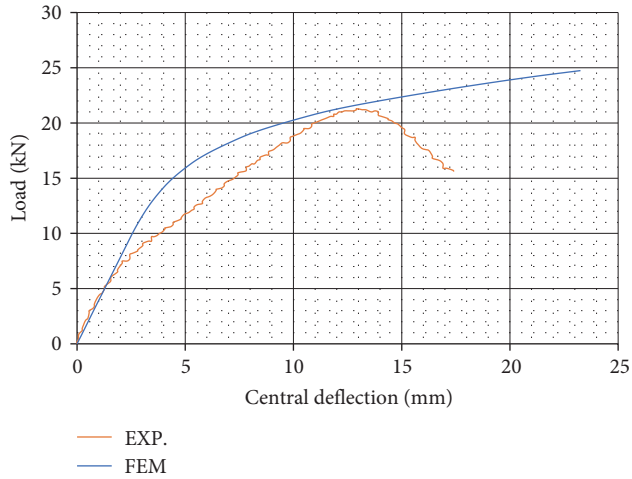

Figure 18: Load–displacement curves' comparison between the FEM and the experimental work results for M2-F4-P5.

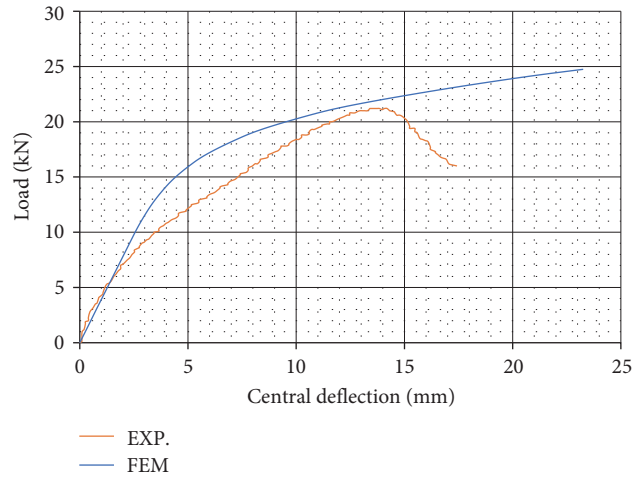

Figure 19: Load–displacement curves' comparison between the FEM and the experimental work results for M3-F4-P10.

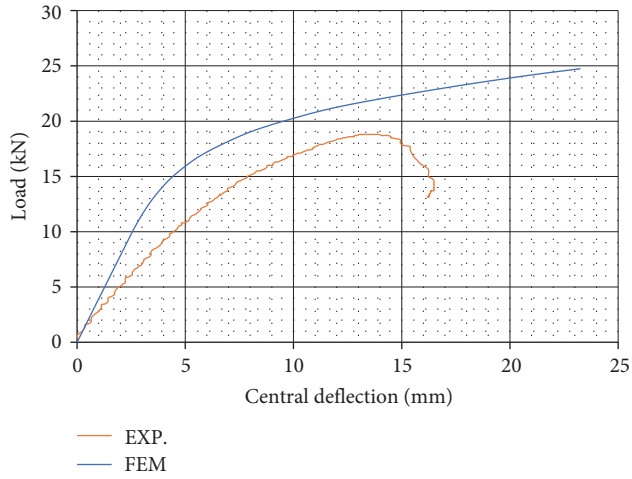

Figure 20: Load–displacement curves' comparison between the FEM and the experimental work results for M4-F4-P15.

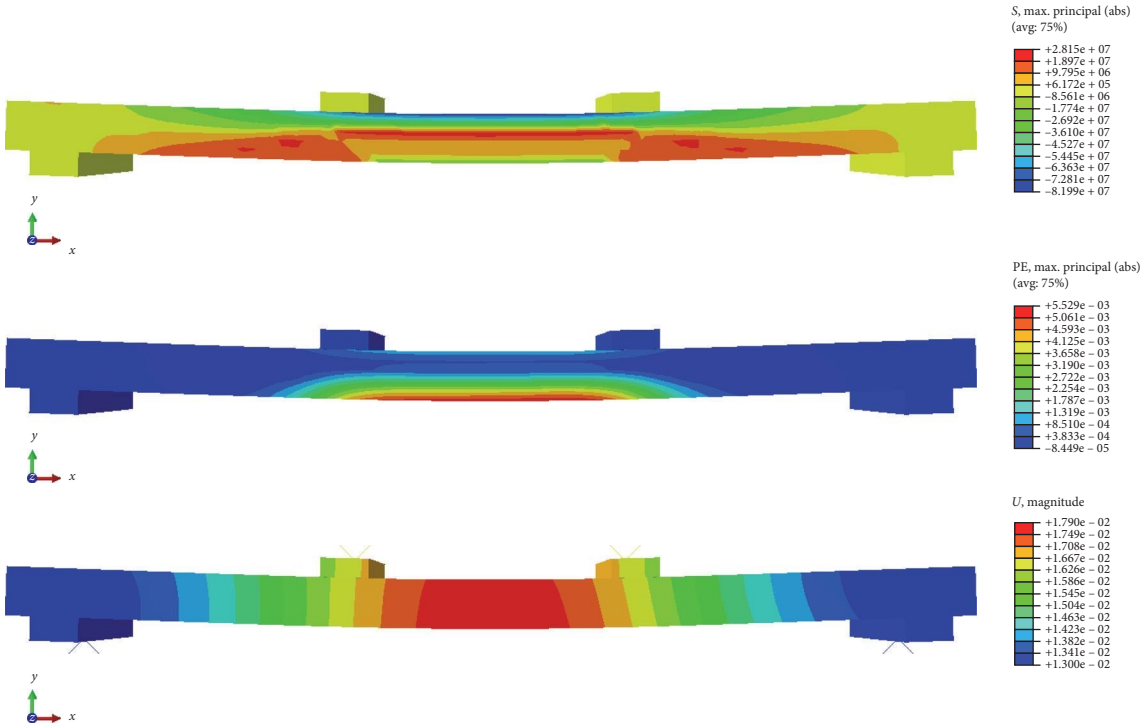

Figure 21: Von Mises stress for the SIFCON plate, plastic strain, and deflection of M1-F4 sample at the maximum load capacity.

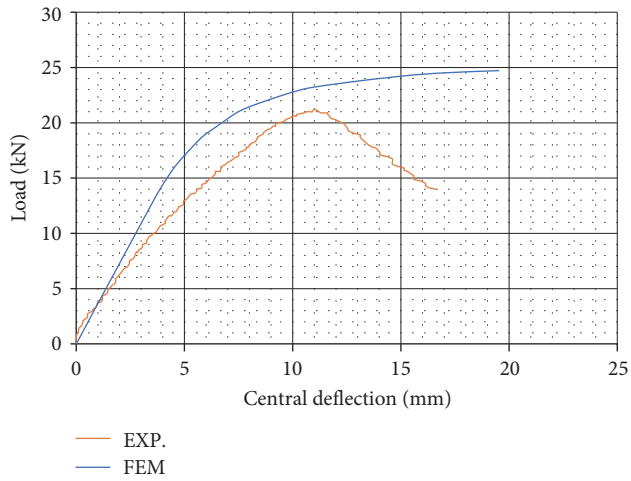

Figure 22: Load–displacement curves' comparison between the FEM and the experimental work results for M1-F4.

5.3. Failure Mode and Visual Observations. The concrete's surface changes can be used to assess the damage caused by prolonged exposure to high temperatures. Checking for concrete surface color change, cracking, and spalling are common visual findings in assessing concrete damage from fire [43]. The specimens were visually evaluated in this study as soon as they were taken out of the furnace. Figure 16 shows the surface of various SIFCON plate specimens following exposure to a 600°C fire flame. In general, the surface color of every SIFCON specimen changed at 600°C, becoming lighter. Also, when heated to 600°C, the powder RPs broke down and lost a lot of mass, turning the surfaces of specimens M2-F4-P5, M3-F4-P10, and M4-F4-P15 brown. Also, after being heated to 600°C, the specimens that contained powder rubber had many holes on their surface because the powder RPs were being removed to the point where light finger pressure would turn the burned powder rubber into powder. It is clear from Figure 12 that SIFCON plates containing powder rubber resist spalling better than the reference specimen M1-F4. This is primarily attributable to the rubber's

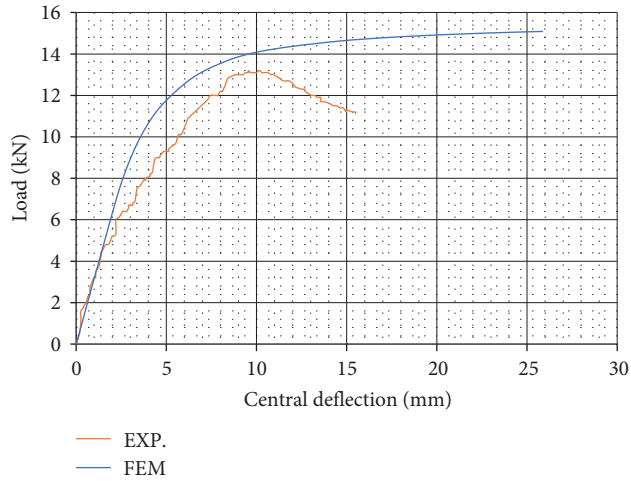

Figure 23: Load–displacement curves' comparison between the FEM and the experimental work results for M2-F4-P5.

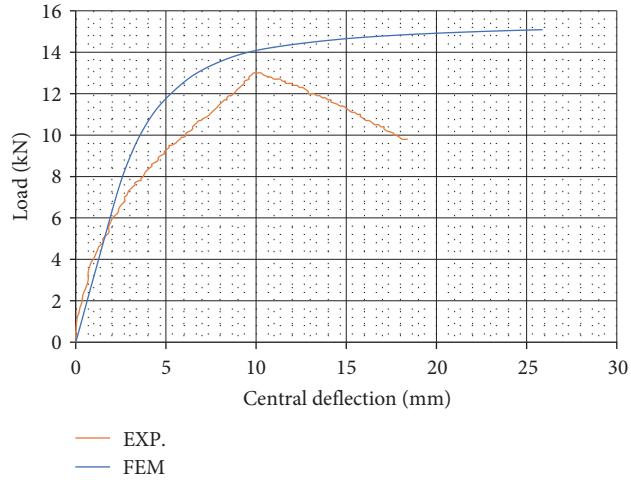

Figure 24: Load–displacement curves' comparison between the FEM and the experimental work results for M3-F4-P10.

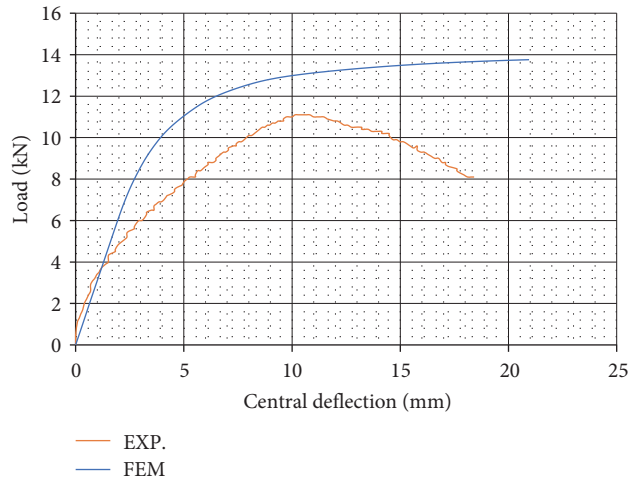

Figure 25: Load–displacement curves' comparison between the FEM and the experimental work results for M4-F4-P15.

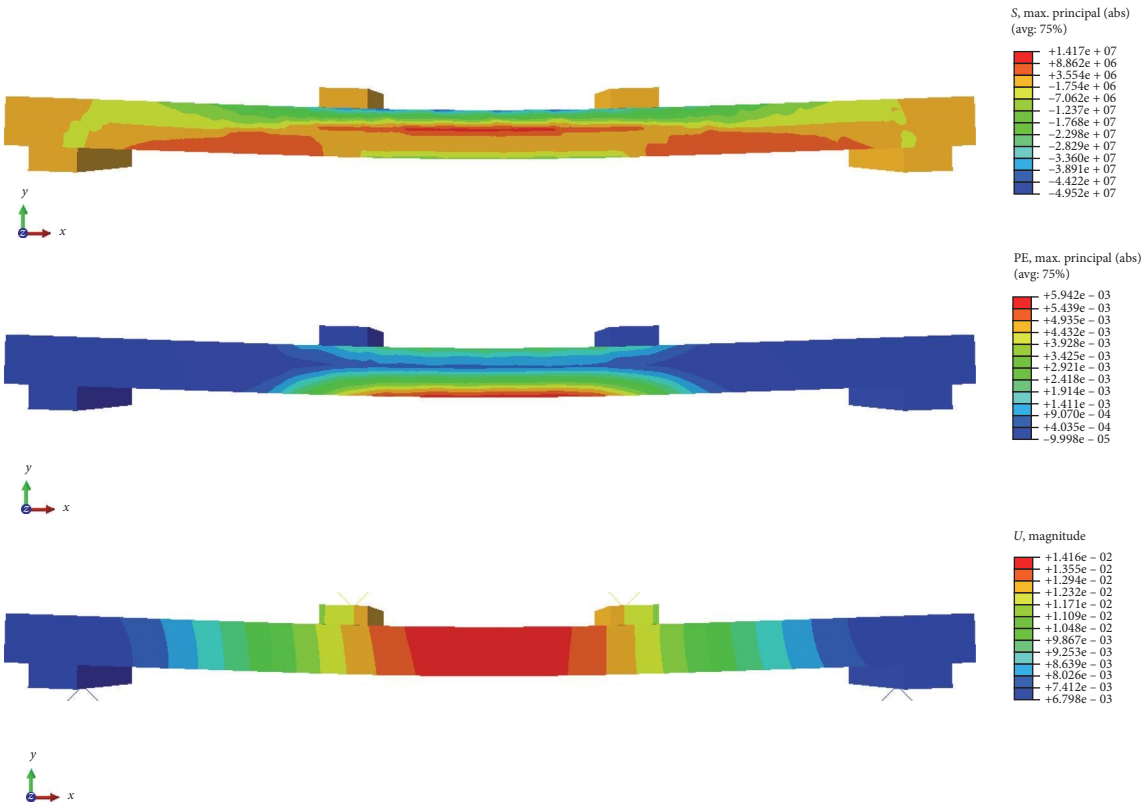

Figure 26: Von Mises stress for the SIFCON plate, plastic strain, and deflection of M2-F4-P5 sample at the maximum load capacity.

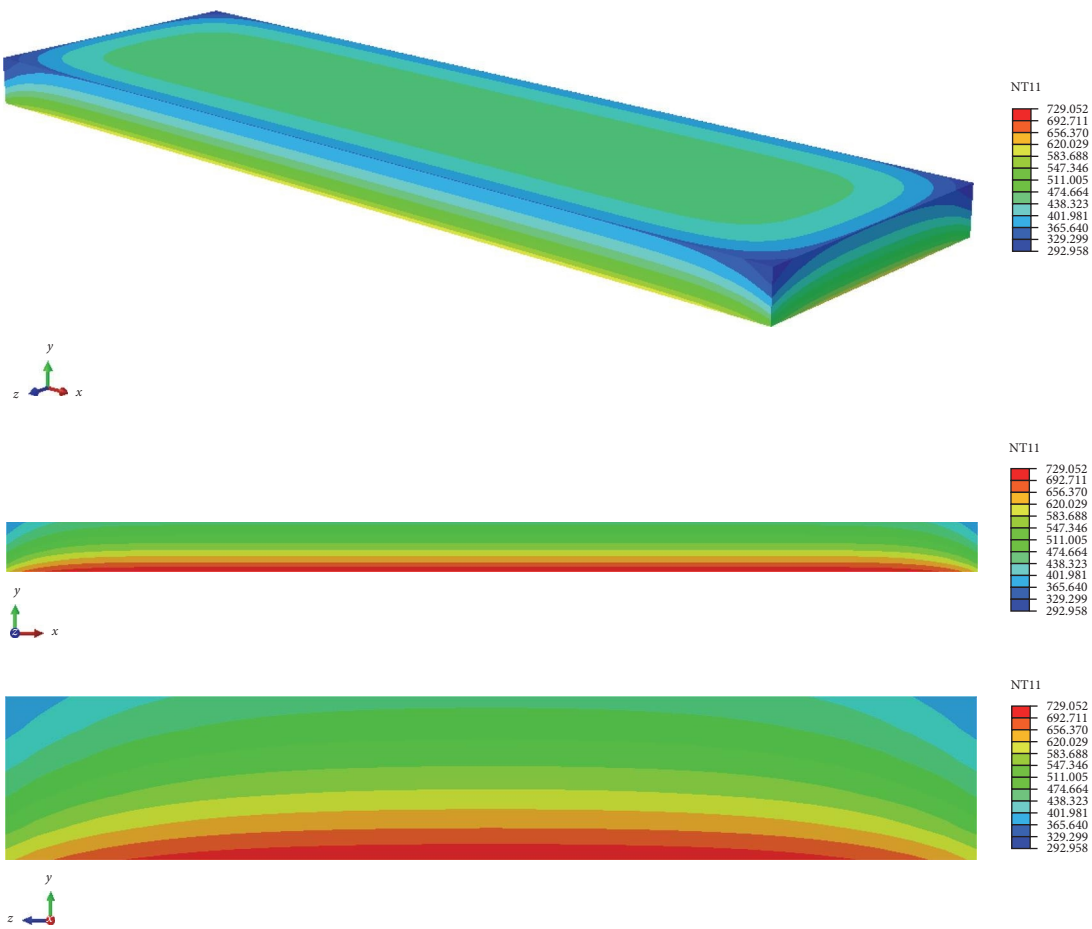

Figure 27: The temperature distribution in the SIFCON plate specimen M1-F4 after burning.

ability to release pore pressure and allow water vapor to escape after melting at 170°C, which minimizes the impact of the pressure on concrete structures [44].

5.4. FEM Results

5.4.1. Results of SIFCON Plates at Ambient Temperatures (25°C). Simulation results of the SIFCON plate specimens before firing are presented in this subsection. As can be seen in Table 8 and Figures 17–20, the load–displacement curves of the experimental and numerical approaches are close to each other for SIFCON plate specimens. The FEM result curve possessed higher initial stiffness than the experimental results. Also, the FEM result reflected a higher load-carrying capacity than the experimental results. Such differences can be accepted, and the adopted parameters can be said to be accurate in this study. The Von Mises stress distribution for the SIFCON plate M1-F4 sample, in addition to the true strain, is illustrated in Figure 21.

5.4.2. FEA Results of SIFCON Plate at Elevated Temperatures (600°C). Figures 22–25 illustrate the measured load-carrying capacity versus the midspan deflection of SIFCON plate specimens based on the numerical and experimental results. From Figures 22–25, a good agreement has been noticed when comparing both the mentioned curves' results. The elastic stage of the FEA results approximately fitted the experimental curve, while slight variations in the inelastic phase have been observed. In addition, it is clear that the midspan displacement corresponded to the maximum load capacity, which was approximately the same. Furthermore, a noticeable variation in the degradation phase was observed. Overall, the percentages of error between the experimental and numerical results for the load capacity and midspan displacement were about 5.05% and 8.65%, respectively. Figure 26 illustrates Von Mises distribution contour map stress, plastic strain, and downward displacement distribution contour maps of the M2-F4-P5 sample, while the computed relations between fire temperatures at different depths from the exposed faces of the M1-F4 plate with time are exhibited in Figure 27.

6. Conclusion

The tests were done on eight one-way plates made of simply supported SIFCON. The plates had different amounts of fine aggregate replaced with recycled powder rubber (0%, 5%, 10%, and 15%). The failure mode of each tested plate was flexure. The initial flexural crack occurred in the middle third of the tension face of the plate, where the maximal moment developed. During the test, the failure of all modified SIFCON plates was observed to be gradual, and the plates remained in contact even after the ultimate load was attained, whereas the failure of the reference mix (without wasted rubber) was observed to be more rapid than that of other SIFCON mixtures. Increasing the powder rubber content of burned and unburned specimens decreases the failure load and increases the specimen's ductility factor, as well as the ultimate and service deflections. Using different grades of waste rubber in the SIFCON mix might lessen this unfavorable effect. Crumb rubber can also be treated with different alkaline chemical compounds to help overcome this performance decline. The use of the techniques mentioned above may be able to increase the bonding between cement paste and waste rubber, leading to an improvement in mechanical and durability properties. Overall, the replacements of 5% and 10% are an efficient and effective mix, and for the flexural test, it gives desirable strength and good fire resistance (modified SIFCON plates containing powder rubber resist spalling better than the reference specimen). It is found from the axial load–displacement relationships that all the theoretical models show a stiffer behavior when compared with the experimental axial load–displacement relationships. Overall, the percentage of error between the experimental and numerical results for the load capacity and midspan displacement was about 5.05% and 8.65%, respectively.

Data Availability

Data for this research article are available upon request.

Conflicts of Interest

The authors declare that they have no conflicts of interest.

Acknowledgments

The authors want to show their appreciation and gratitude to the head and personnel of the University of Technology's Department of Civil Engineering. The authors would also like to express their special appreciation to the staff of the building materials laboratory at the Civil Engineering Department for presenting all the facilities needed to finish this work. Finally, the authors would like to express their gratitude to the Research Square Preprint Server for helping to improve this article before the more formal journal peer review process: https://www.researchsquare.com/article/rs-3326670/v.

References

[1] M. F. Alrubaie, S. A. Salih, and W. A. A. Abbas, "Experimental investigation on protection methods of slurry infiltrated fiber concrete in corrosive environments," in *IOP Conference Series: Materials Science and Engineering*, vol. 737, IOP Publishing, 2020.

[2] A. Bentur and S. Mindess, *Fibre Reinforced Cementitious Composites*, CRC Press, 2006.

[3] A. M. Gilani, *Various durability aspects of slurry infiltrated fiber concrete*, Ph.D.thesis, Middle East Technical University, 2007.

[4] S. Mahadik, S. Kamane, and A. Lande, "Effect of steel fibers on compressive and flexural strength of concrete," *International Journal of Advanced Structures and Geotechnical Engineering*, vol. 3, no. 4, pp. 388–392, 2014.

[5] M. M. Kadhum, A. M. Hashim, S. S. Khamees, A. H. Akhaveissy, and A. H. Ali, "Experimental investigation of fire effects under axial compression on ductility and stiffness of (SIFCON) columns," *Structural Concrete*, vol. 23, no. 6, pp. 3554–3568, 2022.

[6] A. M. Hashim and M. M. Kadhum, "Numerical and experimental study of postfire behavior of concentrically loaded SIFCON

columns," *ACI Structural Journal*, vol. 118, no. 1, pp. 73–86, 2021.

[7] M. Alrubaie, S. Salih, and W. Abbas, "Durability of slurry infiltrated fiber concrete to corrosion in chloride environment: an experimental study, part I," *International Journal of Civil and Environmental Engineering*, vol. 13, no. 8, pp. 502–508, 2019.

[8] D. R. Lankard and D. H. Lease, "Highly reinforced precast monolithic refractories," *American Ceramics Society Bulletin*, vol. 61, no. 7, 1982.

[9] M. M. Kadhum and B. S. Mankhi, "Behavior of reactive powder concrete columns with or without steel ties," *Civil and Environmental Research*, vol. 8, no. 1, 2016.

[10] A. J. Alsaad, T. S. Al-Attar, and B. S. Al-Shathr, "Utilization of mineral sequestration for CO_2 capturing in car parks and tunnels," *Engineering and Technology Journal*, vol. 38, no. 5, pp. 728–737, 2020.

[11] M. M. Al-Tayeb, B. H. A. Bakar, H. Ismail, and H. M. Akil, "Impact resistance of concrete with partial replacements of sand and cement by waste rubber," *Polymer-Plastics Technology and Engineering*, vol. 51, no. 12, pp. 1230–1236, 2012.

[12] T. Gupta, R. K. Sharma, and S. Chaudhary, "Impact resistance of concrete containing waste rubber fiber and silica fume," *International Journal of Impact Engineering*, vol. 83, pp. 76–87, 2015.

[13] K. B. Najim and M. R. Hall, "Mechanical and dynamic properties of self-compacting crumb rubber modified concrete," *Construction and Building Materials*, vol. 27, no. 1, pp. 521–530, 2012.

[14] K. Bisht and P. V. Ramana, "Evaluation of mechanical and durability properties of crumb rubber concrete," *Construction and Building Materials*, vol. 155, pp. 811–817, 2017.

[15] E. Ganjian, M. Khorami, and A. A. Maghsoudi, "Scrap-tyre-rubber replacement for aggregate and filler in concrete," *Construction and Building Materials*, vol. 23, no. 5, pp. 1828–1836, 2009.

[16] F. Rezaeicherati, A. Memarzadeh, A. Esmailpour, H. Fallahnejad, A. Ghorbanzadeh, and M. Nematzadeh, "Durability evaluation and environmental implications of blended cement with colloidal nano-silica for use in recycled fine aggregate concrete: experimental and theoretical study," *Construction and Building Materials*, vol. 402, Article ID 132926, 2023.

[17] M. S. Abdulraheem and M. M. Kadhum, "Experimental investigation of fire effects on ductility and stiffness of reinforced reactive powder concrete columns under axial compression," *Journal of Building Engineering*, vol. 20, pp. 750–761, 2018.

[18] M. K. Al-Khafaji, W. A. Abbas, and S. Al-Mishhadani, "Behavior of high strength concrete containing nano-metakaolin exposure to fire flame," *Engineering and Technology Journal*, vol. 34, no. Issue 5 A, pp. 857–875, 2016.

[19] V. Kodur and T. Harmathy, "Properties of building materials," in *SFPE Handbook of Fire Protection Engineering*, pp. 277–324, Springer, 2016.

[20] M. S. Abdulraheem and M. M. Kadhum, *Effect of fire exposed on the behavior of reactive powder concrete columns under concentric compression loading*, M.S. thesis, University of Babylon, 2017.

[21] V. Kodur and R. Mcgrath, "Fire endurance of high strength concrete columns," *Fire Technology*, vol. 39, no. 1, pp. 73–87, 2003.

[22] P. K. Sarker and S. Mcbeath, "Fire endurance of steel reinforced fly ash geopolymer concrete elements," *Construction and Building Materials*, vol. 90, pp. 91–98, 2015.

[23] D. N. Crook and M. J. Murray, "Regain of strength after firing of concrete," *Magazine of Concrete Research*, vol. 22, no. 72, pp. 149–154, 1970.

[24] J. F. Y. S. Mindess, *Concrete, Prentice-Hall*, New Jersey, USA, Englewood Cliffs, Inc, 1981.

[25] P. Buitelaar, "Heavy reinforced ultra high performance concrete," in *Proceedings of the International Symposium on Ultra High Performance Concrete*, pp. 25–35, Kassel, Germany, 2004.

[26] P. Acker and M. Behloul, "Ductal® technology: a large spectrum of properties, a wide range of applications," in *Proceedings of the International Symposium on Ultra High Performance Concrete*, pp. 11–23, Kassel, Germany, 2004.

[27] A. Beglarigale, Ç. Yalçınkaya, H. Yiğiter, and H. Yazıcı, "Flexural performance of SIFCON composites subjected to high temperature," *Construction and Building Materials*, vol. 104, pp. 99–108, 2016.

[28] F. Hernández-Olivares and G. Barluenga, "Fire performance of recycled rubber-filled high-strength concrete," *Cement and Concrete Research*, vol. 34, no. 1, pp. 109–117, 2004.

[29] A. M. Marques, J. R. Correia, and J. de Brito, "Post-fire residual mechanical properties of concrete made with recycled rubber aggregate," *Fire Safety Journal*, vol. 58, pp. 49–57, 2013.

[30] Y.-C. Guo, J.-H. Zhang, G.-M. Chen, and Z.-H. Xie, "Compressive behaviour of concrete structures incorporating recycled concrete aggregates, rubber crumb and reinforced with steel fibre, subjected to elevated temperatures," *Journal of Cleaner Production*, vol. 72, pp. 193–203, 2014.

[31] F. Aslani and J. Kelin, "Assessment and development of high-performance fibre-reinforced lightweight self-compacting concrete including recycled crumb rubber aggregates exposed to elevated temperatures," *Journal of Cleaner Production*, vol. 200, pp. 1009–1025, 2018.

[32] H. A. Bengar and A. A. Shahmansouri, "Post-fire behavior of unconfined and steel tube confined rubberized concrete under axial compression," *Structures*, vol. 32, pp. 731–745, 2021.

[33] Y. Tang, Y. Wang, D. Wu et al., "Exploring temperature-resilient recycled aggregate concrete with waste rubber: an experimental and multi-objective optimization analysis," *Reviews on Advanced Materials Science*, vol. 62, no. 1, Article ID 20230347, 2023.

[34] A. C150/C150M-18, "ASTM C150/C150M-18," 2018.

[35] ASTM C494/C494M-17, *Standard Specification for Chemical Admixtures for Concrete*, American Society for Testing and Materials International, West Conshohocken, PA, 2017.

[36] A. C1240-15, *Standard Specification for Silica Fume Used in Cementitious Mixtures*, American Society for Testing Materials, 2015.

[37] B. S. Thomas, R. C. Gupta, P. Mehra, and S. Kumar, "Performance of high strength rubberized concrete in aggressive environment," *Construction and Building Materials*, vol. 83, pp. 320–326, 2015.

[38] A. C1437-15, *Standard Test Method for Flow of Hydraulic Cement Mortar*, American Society for Testing Materials, 2015.

[39] W. A. Abdullah, M. R. AbdulKadir, and M. A. Muhammad, "Effect of high temperature on mechanical properties of rubberized concrete using recycled tire rubber as fine aggregate replacement," *Engineering and Technology Journal*, vol. 36, no. 8A, pp. 906–913, 2018.

[40] F. Aslani, G. Ma, D. L. Y. Wan, and G. Muselin, "Development of high-performance self-compacting concrete using waste recycled concrete aggregates and rubber granules," *Journal of Cleaner Production*, vol. 182, pp. 553–566, 2018.

[41] A. H. A. Sabar and M. M. Kadhum, "Numerical modeling of the experimental test for shear strengthened of fire damaged high strength lightweight RC beams with SIFCON jacket," *Periodicals of Engineering and Natural Sciences*, vol. 10, no. 2, pp. 512–538, 2022.

[42] K. H. Tan and H. Zhao, "Strengthening of openings in one-way reinforced-concrete slabs using carbon fiber-reinforced polymer systems," *Journal of Composites for Construction*, vol. 8, no. 5, pp. 393–402, 2004.

[43] A. Baradaran-Nasiri and M. Nematzadeh, "The effect of elevated temperatures on the mechanical properties of concrete with fine recycled refractory brick aggregate and aluminate cement," *Construction and Building Materials*, vol. 147, pp. 865–875, 2017.

[44] L.-J. Li, W.-F. Xie, F. Liu, Y.-C. Guo, and J. Deng, "Fire performance of high-strength concrete reinforced with recycled rubber particles," *Magazine of Concrete Research*, vol. 63, no. 3, pp. 187–195, 2011.